

Short Communication

## Effects of Cobalt(II)Sulfate Addition on Structure and Corrosion Resistance of Alloy Micro-arc oxidation Coating on the ZL108 Aluminum

Jie Hu<sup>1</sup>, Ping Wang<sup>1, 2, 3, \*</sup>, DanDan Liao<sup>1</sup>, XiYue Sun<sup>1</sup>, ZeYu Gong<sup>1</sup>, JiWei Liu<sup>1</sup>, Dan Xiong<sup>1</sup>, Dong Xiang<sup>1</sup>, XiaoTao Zu<sup>2</sup>, XiaoWei Wei<sup>3</sup>

<sup>1</sup> School of New Energy and Materials, Southwest Petroleum University, Chengdu, 610500, China

<sup>2</sup> School of Physics, University of Electronic Science and Technology of China, Chengdu, 611731, China

<sup>3</sup> The Postdoctoral Station at Xihua University Based on Collaboration Innovation Center of Sichuan Automotive Key Parts, School of Materials Science and Engineering, Xihua University, Chengdu, 610039, China

\*E-mail: [818wp@163.com](mailto:818wp@163.com)

Received: 25 February 2020 / Accepted: 8 April 2020 / Published: 10 May 2020

---

Micro-arc oxidation (MAO) coatings were formed on ZL108 aluminum alloy in silicate electrolyte with  $\text{CoSO}_4$ . Scanning electron microscopy (SEM), X-ray diffraction (XRD), X-ray photoelectron spectroscopy (XPS) and electrochemical workstation were used to investigate the effects of  $\text{CoSO}_4$  on the microstructure, phase composition, elemental distribution and corrosion resistance of the MAO coatings. The results showed that the addition of  $\text{CoSO}_4$  increased the micro arc oxidation voltage, which increased the coating formation rate, resulting in an increase in the thickness of the MAO coatings. After the addition of  $\text{CoSO}_4$ , the discharge on the coating surface was more uniform, which made the coating flatter. The phases of the MAO coatings were mainly composed of  $\alpha\text{-Al}_2\text{O}_3$ ,  $\gamma\text{-Al}_2\text{O}_3$  and  $\text{SiO}_2$ . The XPS test results showed that  $\text{CoSO}_4$  was converted to  $\text{CoO}$  and  $\text{Co}_3\text{O}_4$ , which made the MAO coatings denser. Electrochemical corrosion tests showed that the corrosion resistance of the coatings with  $\text{CoSO}_4$  was improved. Therefore, the addition of  $\text{CoSO}_4$  can optimize the structure of the MAO coating and improve its comprehensive properties.

---

**Keywords:** ZL 108 aluminum alloy; Micro-arc oxidation; Cobalt(II)Sulfate; Corrosion resistance

### 1. INTRODUCTION

ZL108 aluminum alloy has been widely used in automobile manufacturing and space because of its high specific strength, low density, low cost, but its low hardness and poor corrosion resistance have been regarded as bottlenecks that restrict its further application [1-2]. Increasing numbers of surface treatments are used to expand the application of ZL 108 aluminum alloys, such as micro-arc oxidation.

Micro-arc oxidation (MAO) is also called plasma electrolytic oxidation or micro-plasma oxidation and can form ceramic coatings on ZL108 aluminum alloy. These ceramic coatings can effectively improve the thickness, microhardness and corrosion resistance of ZL108 aluminum alloy [3-4]. Additionally, micro-arc oxidation is an environmentally friendly and low-cost surface treatment technique. Therefore, it is regarded as a relatively effective surface treatment technology [5-6].

The coating forms on ZL108 aluminum alloy by MAO technology can protect the substrate, but during the process, a lot of discharge micropores remain on the surface of the coatings, which can reduce the density of the coatings, so the protection of the substrate by this method is limited. Therefore, the application of micro-arc oxidation technology to improve the properties of the MAO coatings, such as the corrosion resistance, is worth studying. Adding dopant to the micro-arc oxidation electrolyte to form a coating on ZL108 aluminum alloy is a common method to improve the comprehensive properties of the MAO coatings [7-9]. Jin G et al. [10] found that the addition of  $\text{CoSO}_4$  can enhance the wear resistance of the MAO coatings on the LY12 alloy. Wang P et al. [11] and Wang WB et al. [12] pointed out that adding  $\text{CoSO}_4$  can enhance the corrosion resistance of the MAO coatings on the surface of the magnesium alloy. However, there is no research on the addition of  $\text{CoSO}_4$  to improve the corrosion resistance of MAO coatings on ZL108 aluminum alloy.

In this paper, the effects of  $\text{CoSO}_4$  on micro-arc oxidation voltage, surface morphology, phase composition, element content, microhardness, thickness and corrosion resistance of the micro-arc oxidation coatings on ZL108 aluminum alloy were discussed.

## 2. EXPERIMENTAL PROCEDURE

### 2.1. Coating preparation

ZL108 aluminum alloy was used as the substrate in this experiment. Its main elements and contents (mass percentage) were 0.4~0.9% Mn, 0.5~1.0% Mg, 1.0~2.0% Cu, 11.0~13.0% Si, and the remainder was a balance of Al. The size of the samples was 20 mm×10 mm×2 mm. Before the MAO treatment, the substrate was polished with 600<sup>#</sup>, 1000<sup>#</sup>, 1200<sup>#</sup> and 2000<sup>#</sup> frosted silicon carbide papers, cleaned with distilled water and alcohol, and dried naturally in air.

The MAO process was realized by using a pulsed DC power to offer a positive pulse voltage. The MAO coating was obtained at a fixed frequency of 100 Hz, a duty cycle of 20%, and a current density of 6A/dm<sup>2</sup>. The micro-arc oxidation treatment time of all the samples was 30 mins. The selected electrolyte formulations were:  $\text{Na}_2\text{SiO}_3$  (12 g/L), NaF (1 g/L),  $\text{C}_4\text{H}_4\text{O}_6\text{KNa}$  (2 g/L), and NaOH (3 g/L). In the base electrolyte, the MAO sample was denoted G0.  $\text{CoSO}_4$  (0.8 g/L) was added to the base electrolyte to prepare the modified electrolyte. The MAO sample prepared in the modified electrolyte was denoted G1. The prepared basic electrolyte and modified electrolyte were placed for 24 hours before the MAO treatment to make the ions in the solution more stable. In the process of micro-arc oxidation, the electrolyte temperature was maintained below 30°C and continuously stirred with a blender. When the MAO treatment was finished, the samples were immersed in deionized water at 95°C to seal the treatment for 5 mins and naturally cooled in air.

## 2.2. Microstructural observation and property analysis

The microscopic morphology of the coating was observed by scanning electron microscopy (SEM, ZEISS EVO MA15, Germany), and the distributions of Co, Al, O and Si on the surface of the MAO coatings were determined by X-ray energy dispersive spectrometry (EDS, OXFORD 20, America). X-ray diffraction (XRD, DX-2700B, China) was used to analyze the composition of the phase in the MAO coatings. The diffraction data was acquired with scattering angle  $2\theta$  from  $10^\circ$  to  $80^\circ$ , and scanning speed was  $0.04^\circ/\text{s}$ . X-ray photoelectron spectroscopy (XPS) was used to analyze the chemical states of Co in the MAO coatings. The surface microhardness was measured by a digital microhardness tester (HXD-2000TM/LCD, China) with load of 1 N for 15 s. Five regions were measured for each micro-arc oxidation coating, and the average value was the microhardness of the coatings. The thickness of the coating was measured by an eddy current thickness gauge (TT230, China). Five data were measured for each micro-arc oxidation coating and the average value was the thickness of the coatings.

At room temperature, an electrochemical workstation (Gamry Reference 3000, America) was used to obtain polarization curves and electrochemical impedance spectroscopy (EIS) in the 3.5% NaCl solution. The reference electrode (RE) was a saturated calomel electrode, and the auxiliary electrode (CE) was a platinum electrode. The surface area of the sample exposed to NaCl solution was  $0.5\text{cm}^2$ . The sample was used as the working electrode. To ensure the solution reached a stable state, the samples were soaked in NaCl solution for an hour before each test. The scanning rate of the polarization tests was  $0.1\text{ mV s}^{-1}$  and the potential ranged from  $-1.7\text{ V}$  to  $-1.3\text{ V}$  according to the open circuit potential (OCP) of  $-1.6\text{ V}$ . The EIS tests were performed in the frequency range of 100 kHz to 0.01 Hz.

## 3. RESULTS AND DISCUSSION

### 3.1 Voltage-time curves

Figure 1 shows the relationship between voltage-time curves of G0 and G1 coatings. It is obvious that the voltage growth rate of G1 exceeded that of G0. During the process, the micro-arc oxidation voltage of G1 was higher than that of G0. This occurred because  $\text{CoSO}_4$  was easily adsorbed on the ZL108 aluminum alloy surface, so the potential barrier between the ZL108 aluminum alloy and an electron avalanche easily occurred, which promoted "electric breakdown" [13]. The more easily electron avalanche occurs, the faster the coating formation rate. Therefore, the thickness of the coating was increased. The electric resistance of the coating increased, which resulted in an increase in voltage.

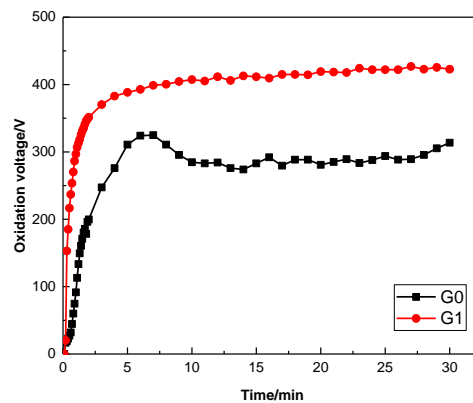


**Figure 1.** Voltage-time curves of G0 and G1.

3.2 The surface and cross-section morphologies of the coatings

According to the observations in Fig. 2 ((a) and (c)), when  $\text{CoSO}_4$  was added to the electrolyte, the surface morphology of the coatings changed significantly: the size and the number of the discharge micropores in the coatings decreased. The porosity and wavy bumps around the discharge micropores were reduced. On the one hand,  $\text{CoSO}_4$  was adsorbed on the surface of the coatings, which can form a discharge center.

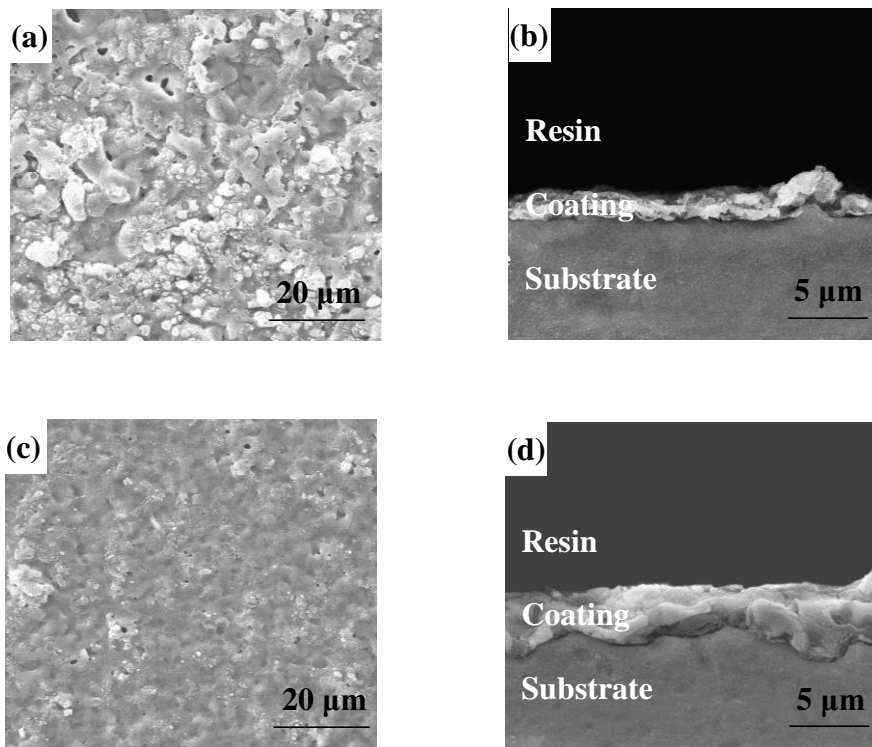


**Figure 2.** Surface and cross-section morphologies of the MAO coatings ((a),(b): G0; (c),(d): G1)

Therefore, the discharge on the surface of the coatings was more uniform [14]. On the other hand,  $\text{CoSO}_4$  can be adsorbed in the discharge micropore channels, filling the discharge micropores were [15]. As a result, the coatings became flatter and denser. Table 1 shows the contents of Co, Al, O and Si in the coatings of G0 and G1. According to the previous study, the addition of  $\text{CoSO}_4$  accelerated the micro-arc oxidation reaction, thus promoting the combination of  $\text{Al}^{3+}$  and  $\text{O}^{2-}$ . Therefore, the Al content on the surface of the coating increased. Moreover, it can be clearly seen that no Co was found in G0, but Co was detected in G1. It is obvious that the Co originated from  $\text{CoSO}_4$ . In summary, adding  $\text{CoSO}_4$  to the electrolyte is a feasible reasonable and promising method for making the surface flatter and denser.

Observation of the cross-section morphology of the MAO coatings in Fig. 2 ((b) and (d)) shows that the thickness and compactness of the coatings increased when  $\text{CoSO}_4$  was added, which was consistent with the previous analysis.

**Table 1.** The contents of Al, Si, O and Co in the coating

Atomic%	G0	G1
Al	50.03	67.16
Si	5.65	0.85
O	44.32	31.81
Co	—	0.18

### 3.3 Phase compositions of the MAO coatings and XPS analysis

As it can be seen from the Fig. 3, the phases of the MAO coatings were mainly composed of  $\gamma\text{-Al}_2\text{O}_3$ ,  $\alpha\text{-Al}_2\text{O}_3$  and  $\text{SiO}_2$ . The main peak of Al can be detected because X-ray rays can penetrate the substrate through the MAO coating. The phase of  $\text{SiO}_2$  mainly came from  $\text{Na}_2\text{SiO}_3$  in the electrolyte. Due to the local high temperature, amorphous  $\text{Al}_2\text{O}_3$  gradually transformed to  $\gamma\text{-Al}_2\text{O}_3$  and  $\alpha\text{-Al}_2\text{O}_3$ .

To verify the presence of Co in the micro-arc oxidation coatings, X-ray photoelectron spectroscopy was performed on the coating with  $\text{CoSO}_4$ . Figure 4 (a) and (b) represent the full XPS and  $\text{Co}2\text{p}$  XPS spectra, respectively. From Fig. 4, it is clear that the  $\text{Co}2\text{p}$  spectrum was split into two peaks ( $\text{Co}2\text{p}_{3/2}$  and  $\text{Co}2\text{p}_{1/2}$ ). Some studies showed that the binding energies of 780.3 eV for  $\text{Co}2\text{p}_{3/2}$  and 797.6 eV for  $\text{Co}2\text{p}_{1/2}$  are  $\text{Co}_3\text{O}_4$  [16-17]. The peak binding energies of 781.2 eV for  $\text{Co}2\text{p}_{3/2}$  and 796.2 eV for  $\text{Co}2\text{p}_{1/2}$  mainly correspond to  $\text{CoO}$  [18]. Thus, Co successfully entered the MAO coatings and existed in form of  $\text{Co}_3\text{O}_4$  and  $\text{CoO}$ .

Furthermore, because the electrolyte contained  $\text{NaOH}$  (3 g/L), it can produce  $\text{OH}^-$ , which could be combined with  $\text{Co}^{2+}$  in the system to form  $\text{Co}(\text{OH})_2$  (see Eq. (1)). Then, as the  $\text{Co}(\text{OH})_2$  was unstable,  $\text{O}^{2-}$  was produced during micro-arc oxidation and can oxidize  $\text{Co}(\text{OH})_2$  into  $\text{Co}_3\text{O}_4$ . On the other hand, the high temperature of micro-arc oxidation can decompose  $\text{Co}(\text{OH})_3$  into  $\text{CoO}$ . It can be determined that  $\text{Co}_3\text{O}_4$  changed to  $\text{CoO}$  during micro-arc oxidation (see Eq. (3)) by referring to the Lange's Handbook of Chemistry [19]. However,  $\text{Co}_3\text{O}_4$  was only partially oxidized to  $\text{CoO}$ . Therefore, there were both  $\text{Co}_3\text{O}_4$  and  $\text{CoO}$  in the micro-arc oxidation coatings. Through the analysis, the possible reactions that occurred during the MAO process were as follows [11]:

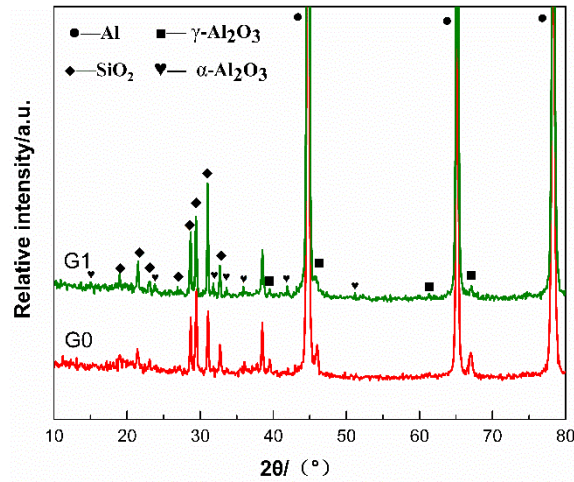
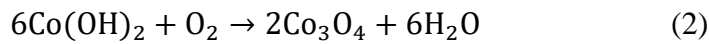
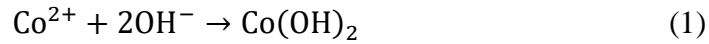


Figure 3. XRD spectra of the MAO coating of G0 and G1.

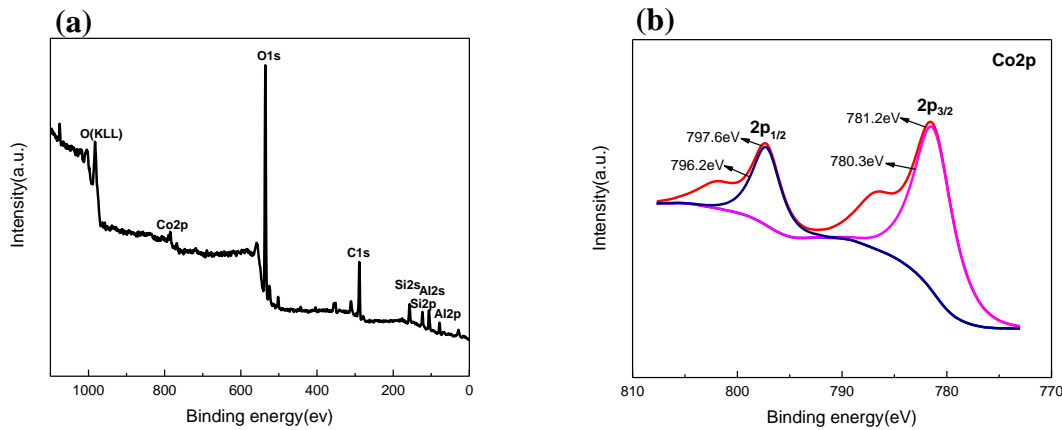
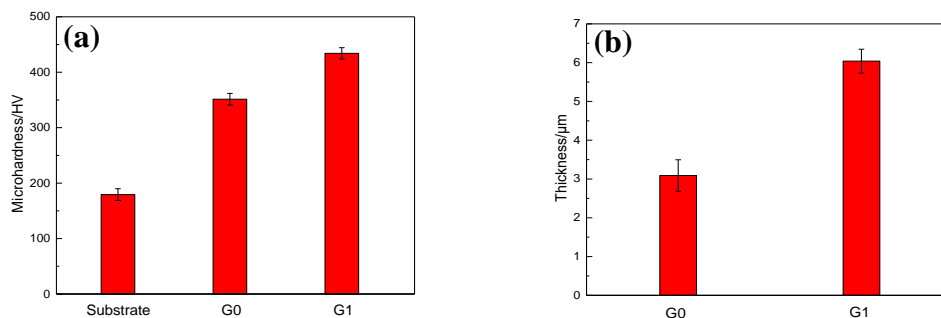


Figure 4. XPS spectra of the MAO coating of the G1 sample.

### 3.4 The microhardness and thickness of the MAO coatings

As shown in Fig. 5, the microhardness and thickness of the MAO coating increased when  $\text{CoSO}_4$  was added. The microhardness of the coatings was related to the thickness, compactness and phase composition. First, the coating thickness increased with the addition of  $\text{CoSO}_4$ . Second, the compactness of the MAO coatings was related to the Pilling-Bedworth ratio (PBR) [20]. When the PBR value of the MAO coatings is greater than 1, the compressive stress of the metal oxidation coating increases with the increase of the value, and the protective effect of the coating is enhanced. A study showed that the PBR value of  $\text{Al}_2\text{O}_3$  is 1.28 and that of  $\text{Co}_3\text{O}_4$  is 1.99 [21]. Therefore, the oxidation coating containing  $\text{Co}_3\text{O}_4$  was denser than that without  $\text{Co}_3\text{O}_4$ . Third, Student MM et al. [22] and Shi L et al. [23] demonstrated

that the  $\gamma\text{-Al}_2\text{O}_3$ ,  $\alpha\text{-Al}_2\text{O}_3$  and  $\text{SiO}_2$  in the coating exhibited high hardness. In summary, when  $\text{CoSO}_4$  was added, the microhardness and thickness of the MAO coatings increased.



**Figure 5.** The microhardness and thickness of MAO coatings ((a): the microhardness, (b): the thickness).

### 3.5 The corrosion resistance of the MAO coatings

Figure 6 shows the Nyquist plots and Bode plots of the ZL108 aluminum alloy substrate and the two MAO coatings (G0 and G1). From Fig. 6 (a), it can be concluded that the arc radii of coatings G0 and G1 were larger than that of the substrate, which meant that the corrosion resistance of the coating treated with micro-arc oxidation was improved [24]. The arc radius of the coating G1 was larger than that of G0 indicating that the corrosion resistance of micro-arc oxidation coating was further improved by adding  $\text{CoSO}_4$ . Through the observation and analysis of the Bode curves in Fig. 6(b) and (c), it can be found that the sample with the MAO coating had higher impedance value than the ZL108 aluminum alloy substrate. The higher the impedance modulus, the better the corrosion resistance [25]. With the addition of  $\text{CoSO}_4$ , the corrosion resistance of the MAO coating was significantly improved. Because the two time constants can be determined from Fig. 6(c), the electrical equivalent circuit can be proposed to quantitatively analyze the impedance value, as shown in Fig. 6(d). In the equivalent circuit,  $R_s$  is the resistance of the solution.  $R_1$  and  $R_2$  are the resistance of outer layer and inner layer of the MAO coatings. CPE1 and CPE2 are the constant-phase element of the outer layer and the inner layer of the MAO coatings. EIS data of different samples were fitted using the model, and the fitting results are represented in Table 2. In Table 2, the resistance value of coating G1 ( $R_1$  and  $R_2$ ) was larger than that of G0. This was due to the denser surface and low porosity of coating G1. Moreover, the closer  $n$  is to 1, the denser the coatings [26]. Both the CPE1 and CPE2 of the coating G1 were smaller than those of the coating G0, which meant that the corrosion resistance of the coating was greatly enhanced with the addition of  $\text{CoSO}_4$ . EIS test results showed that the addition of  $\text{CoSO}_4$  can improve the thickness and compactness of the MAO coatings, which helped prevent the substrate from  $\text{Cl}^-$  immersion and corrosion, so the corrosion resistance of the MAO coatings with  $\text{CoSO}_4$  was significantly improved.

The potentiodynamic polarization curves of the MAO coatings and ZL108 aluminum alloy substrate in 3.5 wt% NaCl solution are shown in Fig. 7. The corrosion potential ( $E_{\text{cor}}$ ) and corrosion current density ( $i_{\text{corr}}$ ) were directly derived from the potentiodynamic polarization curves by Tafel region extrapolation. The parameters obtained from the polarization curve are displayed in Table 3. It can be concluded from the data in Table 3 that compared with the ZL108 aluminum alloy substrate, the

MAO coatings (G0 and G1) had lower self-corrosion currents, and the corrosion rate of the MAO coatings was lower than that of the substrate, which indicated that MAO coatings had better corrosion resistance than the ZL108 aluminum alloy substrate, especially, the MAO coating with  $\text{CoSO}_4$ . In other words, with the addition of  $\text{CoSO}_4$ , the corrosion resistance of the MAO coatings can be effectively improved. This result was consistent with previous EIS test results.

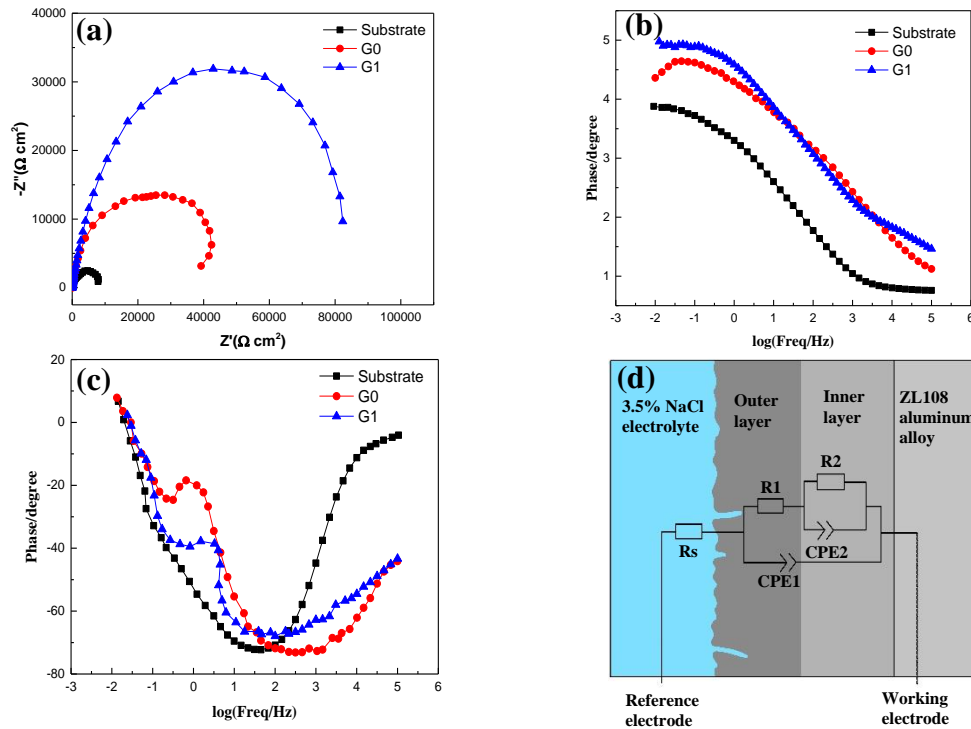


**Figure 6.** EIS spectra of the ZL108 aluminum alloy substrate and the two MAO-coated samples: (a) Nyquist plots; (b, c) Bode plots; (d) equivalent circuit.

**Table 2.** Electrochemical parameters obtained from EIS spectra of MAO coatings

Sample	$R_s$ ( $\Omega \cdot \text{cm}^2$ )	$\text{CPE1}$ ( $\Omega^{-1} \cdot \text{cm}^{-2} \text{S}^n$ )	$n_1$	$R_1$ ( $\Omega \cdot \text{cm}^2$ )	$\text{CPE2}$ ( $\Omega^{-1} \cdot \text{cm}^{-2} \text{S}^n$ )	$n_2$	$R_2$ ( $\Omega \cdot \text{cm}^2$ )
Substrate	7.323	1.276E-5	0.68	5.426E+3	4.337E-4	0.66	4.825E+3
G0	8.629	2.685E-6	0.77	1.496E+4	5.352E-5	0.76	2.857E+4
G1	13.81	1.672E-6	0.81	3.371E+5	2.759E-6	0.84	8.497E+5

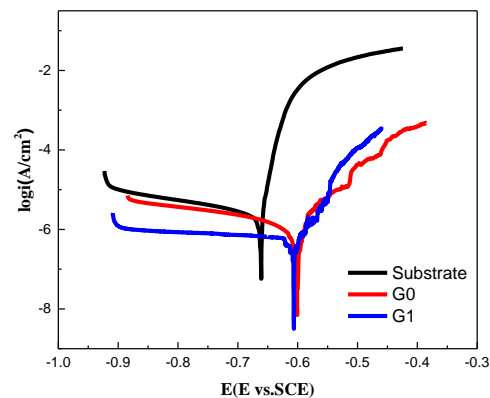


**Figure 7.** Polarization curves of the ZL108 aluminum alloy substrate and the two MAO-coated samples.

**Table 3.** Electrochemical data from the polarization tests for ZL108 aluminum alloy substrate and the two MAO-coated samples.

Sample	$E_{\text{corr}}/\text{V}$	$I_{\text{corr}}/(\text{A}/\text{cm}^2)$	Corrosion rate/(mm/a)
Substrate	-0.687	$3.59 \times 10^{-5}$	$4.88 \times 10^{-1}$
G0	-0.611	$6.28 \times 10^{-7}$	$4.25 \times 10^{-2}$
G1	-0.607	$5.68 \times 10^{-8}$	$7.37 \times 10^{-3}$

#### 4. CONCLUSIONS

(1) The addition of  $\text{CoSO}_4$  can improve the micro-arc oxidation voltage and promote the micro-arc oxidation reaction. The coating formation rate and the coating thickness were increased.

(2) The addition of  $\text{CoSO}_4$  increased the MAO coatings thickness and microhardness. XRD analysis showed that  $\gamma\text{-Al}_2\text{O}_3$ ,  $\alpha\text{-Al}_2\text{O}_3$  and  $\text{SiO}_2$  were the main phases. The analysis of the XPS spectrum proved that  $\text{CoO}$  and  $\text{Co}_3\text{O}_4$ , which made the coating denser, were present in the MAO coating with  $\text{CoSO}_4$ . The SEM morphologies indicated that the surface and cross-section morphology of the MAO coatings became flatter and denser when  $\text{CoSO}_4$  was added.

(3) The corrosion resistance of the coatings was improved with the addition of  $\text{CoSO}_4$ . The impedance values of the outer layer and the inner layer of the MAO coating with  $\text{CoSO}_4$  in the EIS were  $3.371 \times 10^5 (\Omega/\text{cm}^3)$  and  $8.497 \times 10^5 (\Omega/\text{cm}^3)$ , which were an order of magnitude higher than those of the outer layer and the inner layer without  $\text{CoSO}_4$ . The corrosion rates of the polarization curves of the substrate and the MAO coatings G0 and G1 were  $4.88 \times 10^{-1} \text{ A}/\text{cm}^2$ ,  $4.25 \times 10^{-2} \text{ A}/\text{cm}^2$ , and  $7.37 \times 10^{-3} \text{ A}/\text{cm}^2$ , respectively.

## ACKNOWLEDGMENT

The project was funded by China Postdoctoral Science Foundation (2019M663470).

The present work was supported by the Open Fund of Sichuan Province University Key Laboratory of oil and gas field material (grant number X151519KCL06), Southwest Petroleum University.

## DECLARATION OF INTEREST

The authors declare that there are no conflicts of interest regarding the publication of this paper.

## References

1. J.L. Xu , F. Liu , F.P. Wang, D.Z. Yu and L.C. Zhao, *J. Alloy. Compd.*, 472(2009)276.
2. Y. Wang, D.B. Wei, J. Yu and S.C. Di, *J. Mater. Sci. Technol.*, 30(2014)984.
3. Y. Han, S.H. Hong and K.W. Xu, *Surf. Coat. Technol.*, 168(2003)249.
4. P. Wang, T. Wu, Y.T. Xiao, L. Zhang, J. Pu, W.J. Cao and X. M. Zhong, *Vacuum.*, 142(2017)21.
5. M. Fazel, H.R. Salimijazi, M.A. Golozar and jazi. Garsivaz, *Appl. Surf. Sci.*, 324(2015)751.
6. P. Wang, T. Wu, Y.T. Xiao, J. Pu, X.Y. Guo, J. Huang and C.L. Xiang, *J. Mater. Eng. Perform.*, 25(2016)3972.
7. S. Wei, L.Y. Zhou, Q.W. Yu and F.W. Xu, *Adv. Mater. Res.*, 900(2014)522.
8. P. Wang, T. Wu, Y.T. Xiao, J. Pu and X.Y. Guo, *Mater. Lett.*, 182(2016)27.
9. D. Huang, X.Y. Zhang, D.F. Wu and X.S. Zhou, *Adv. Mater. Res.*, 850-851(2014)140.
10. G. Jin, Y.H. Li, G. Zhang, Y.G. Mu and J. Yao, *Heat. Treat. Met.*, 34(2009)61.
11. P. Wang, Z.Y. Gong, H.L. Li, Q.G. Yang, W.J. Cao, J. Hu, J. Pu, X.Y. Guo and D. Xiang, *Surf. Eng.*, 36(2020)216.
12. W.B. Wang, F.Q. Xie and X.Q. Wu, *Mater. Prot.*, 44(2011)45.
13. Q.Z. Chen, Z.Q. Jiang, S.G. Tang, W.B. Dong, Q. Tong and W.Z. Li, *Appl. Surf. Sci.*, 423(2017)939.
14. J.M. Albella, I. Montero and J.M. Martinez-Duart, *Cheminform.*, 131(1984)1101.
15. H.F. Guo and M.Z. An, *Appl. Surf. Sci.*, 252(2006)7911.
16. F. Hong, M.F. Wang and Y.H. Ni, *J. Clust. Sci.*, 29(2018)663.
17. N.S. McIntyre, D.D. Johnston, L.L. Coatsworth, R.D. Davidson and J.R. Brown, *Surf. Interface. Anal.*, 15(2010)265.
18. S. Kundu, M.D. Mukadam, S.M. Yusuf and M. Jayachandran, *Crystengcomm.*, 15(2013)482.
19. J.A. Dean, *Adv. Manufacturing. Pro.*, 5(2007)687.
20. L. Arurault, *Inter. J. Sur. Eng. Coat.*, 86(2013)51.
21. C. Xu and W. Gao, *Mater. Res. Innov.*, 3(2000)231.
22. M.M. Student, V.M. Dovhnyk, M.D. Klapkiv, V.M. Posuvailo, V.V. Shmyrko and A.P. Kytsya, *Mater. Sci.*, 48(2012)180.
23. L. Shi, C.F. Sun, P. Gao, F. Zhou and W.M. Liu, *Appl. Surf. Sci.*, 252(2006)3591.
24. H.J. Ma, D.L. Li, C. Liu, Z.Q. Huang, D.L. He, Q. Yan, P. Liu, Philip.Nash and D.J. Shen, *Surf. Coat. Technol.*, 266(2015)151.
25. Q.Z. Chen, Z.Q. Jiang, S.G. Tang, W.B. Dong, Q.T. and W.Z. Li, *Appl. Surf. Sci.*, 423(2017)939.
26. W.Y. Liu, Y. Liu, Y.H. Lin, Z. Zhang, S.B. Feng, Mohd. Talha, Y.S. Shi and T.H. Shi, *Appl. Surf. Sci.*, 475(2019)645.